Convenient Synthesis of Hybrid Polymer Materials by AGET-ATRP Polymerization of Pickering Emulsions Stabilized by Cellulose Nanocrystals Grafted with Reactive Moieties

Arthur Werner, Véronique Schmitt, Gilles Sèbe, Valérie Héroguez

CONVENIENT SYNHTESIS OF HYBRID POLYMER MATERIALS BY AGET-ATRP POLYMERIZATION OF PICKERING EMULSIONS STABILIZED BY CELLULOSE NANOCRYSTALS GRAFTED WITH REACTIVE MOIETIES

Arthur Werner[†*], *Véronique Schmitt*[§], *Gilles Sèbe*[†], *Valérie Héroguez*[†*].

[†]Laboratoire de Chimie des Polymères Organiques CNRS UMR5629, IPB-ENSCBP, Université de Bordeaux, 16 avenue Pey-Berland, F-33600 Pessac, France.

[§]Centre de Recherche Paul Pascal UMR 5031 CNRS Université de Bordeaux, 115 Avenue du Dr Albert Schweitzer, 33600 Pessac, France

Cellulose nanocrystals, CNC, Pickering Emulsion, Polymerization, AGET ATRP, direct, inverted, double.

Abstract

We report a novel method to prepare capsules, beads or open-cell materials from Pickering emulsions of monomers, stabilized by cellulose nanocrystals (CNCs) grafted with reactive Isobutyrate bromide moieties (CNC-Br). CNC-Br particles with different hydrophylic/hydrophobic balance at their surface were prepared, and subsequently used to stabilize direct (O/W), inverted (W/O), or double emulsions of Styrene or *n*-BuA. The different emulsions obtained were subsequently polymerized, by initiating an AGET-ATRP polymerization from the brominated particles surrounding the stabilized droplets. The different hybrid polymer materials obtained were subsequently characterized, and the impact of the CNCs functionalization and polymerization conditions was particularly discussed.

Introduction

Cellulose NanoCrystals (CNCs) are biosourced, biorenewable, needle shaped nanoparticles measuring typically 50-350 nm in length and 5-20 nm in width.[1] Commonly extracted from cellulose substrates by acid treatment, they are decorated by anionic sulfate ester groups at their surface and exhibit unique properties widely documented in the literature.[1–4] In particular, the possibility of using them as emulsifiers in Pickering emulsions has gained increasing attention in recent years.[5–8] The high stability of such emulsions is well known, and relies on the irreversible adsorption of the nanoparticles at oil-water interfaces, without need of additional surfactant.[9] For this reason, these green Pickering emulsifiers are now attracting the interest of various industries in area as diverse as food, cosmetics or paint. Although direct oil-in-water emulsions (O/W) can be easily stabilized with pristine CNCs,[10–14] the chemical functionalization of the particles surface

offers the possibility to prepare various types of emulsions including direct (O/W)[15], inverted (W/O),[16,17] and double emulsions (O/W/O or W/O/W).[18] Recently, it has been shown that Pickering emulsions could be also used as a radical polymerization vessels for the production of composite lattices composed of polymer beads decorated by the stabilizing nanoparticles.[19–22] In particular, we recently reported the successful preparation and radical polymerization of a wide range of O/W Pickering emulsions prepared with different monomers and stabilized by CNCs grafted with acetyl groups at their surface.[23] The monomer droplets were easily polymerized without destabilization, leading to the production of micro or nanolatex covered by the acetylated nanoparticles. In these experiments, the radical initiator was solubilized in the oil phase. Polymerization from initiating sites immobilized at the CNCs surface could be also envisaged.[24–27] Depending on whether the polymerization is initiated from the inner[28,29] or outer[30] surface of the Pickering particles, capsules or hairy particles can be respectively obtained.[30]

In this paper, we present the stabilization of Pickering direct, inverted and double emulsions of styrene or *n*-BuA monomers, using CNC particles grafted with reactive Isobutyrate bromide moieties. The different emulsions obtained were subsequently polymerized, by initiating an AGET-ATRP reaction from the brominated particles surrounding the stabilized droplets. The different polymer materials obtained (capsules, beads or open-cell solids) were subsequently characterized, and the impact of the CNCs functionalization and polymerization conditions was studied.

Materials

The unmodified CNCs used in this study were isolated by sulfuric acid hydrolysis of wood pulp, according to a general procedure widely described in the literature.[31] The initial nanoparticles had a rod-like shape with estimated dimensions of 130 ± 43 nm in length and 18 ± 3 nm in diameter, based on AFM topography images (SI, Figure S1). In aqueous suspension, the CNCs displayed a zeta potential of –33.1 mV consistent with the presence of negative sulfate ester groups at their surface, as expected after the sulfuric acid treatment. A surface OH content of 3.10 mmol.g^{-1}, (corresponding to 16.7 mol% of the total OH groups contained in the CNCs) was estimated in a previous study.[32]

Acetylated CNCs (CNCAs$_9$) with a grafting level corresponding to the substitution of 9% of the total OH groups were synthetized, following a previously established protocol.[7]

Styrene (St) (Sigma Aldrich, >99%), *n*-Butyl Acrylate (*n*-BuA) (Sigma Aldrich, 99%) were purified on alumina column to remove trace of stabilizers. Vinyl acetate (VAc)(Sigma Aldrich, 99%), 2-Bromoisobutyryl bromide (Bibb) (Alfa Aesar, 97%), Ethyl bromoisobutyrate (Ebib) (Sigma Aldrich, 98%), Ascorbic acid (ABCR, 99%), Copper(II) bromide ($CuBr_2$) (ABCR, 99%), 4-Dimethylaminopyridine (DMAP) (TCI, >99%), Triethylamine (TEA) (Sigma Aldrich, 98%), 2-(Chloromethyl)pyridine hydrochloride (ABCR, 98%), Octadecylamine (ABCR, 97%), NaOH (TCI, 99%), Succinic anhydride (ABCR, 99%), N,N,N',N'-tetramethyl-O-(1H-benzotriazol-1-yl)uronium hexafluorophosphate (HBTU) (Sigma Aldrich, 99%), N,N-Diisopropylethylamine (DIEA) (Sigma Aldrich, 99%), Fluoresceine cadaverine (FC) (VWR, 99%) were used without further purification.

Solvent were purchased at VWR (DMF, DMSO, Methanol, THF, Diethylether, DCM, Cyclohexane, Ethyl acetate, analysis grade), DMF and DMSO were purified on column, others were used without purification.

The ligand bis(2-pyridylmethyl)octadecylamine (BPMODA) was synthetized by following the protocol of Matyjaszewski et al.[33]

Equipments and methods

Infrared spectra of the acetylated and unmodified CNCs were recorded using a Vertex 70 Brüker FT-IR spectrometer. For each sample, the diamond crystal of an attenuated total reflectance (ATR) accessory was brought into contact with the area to be analyzed. All spectra were recorded between 4 000 and 400 cm^{-1} with a resolution of 4 cm^{-1} with 32 scans per sample.

Nuclear Magnetic Resonance (NMR) spectra were recorded on a Bruker Avance 400 (^1H at 400,2 MHz) in deuterated chloroform ($CDCl_3$) solvent with t_{relax} = 1 second and n_{scan} = 16.

Steric Exclusion Chromatography (SEC) was performed in tetrahydrofuran (THF) (1mL/min) with trichlorobenzene as flow marker equipped with refractometric, light scattering and UV detectors.

Scanning electron microscopy (SEM) observations were performed with a HITACHI TM-1000 apparatus operating at 15 kV and samples were metallized 90 seconds with platinum plasma at 10 mA before observation.

Cryo–Scanning Electron Microscopy (Cryo-SEM) analysis were carried out using a SEM-FEG HR (JEOL 6700F) apparatus. 500 µL of the emulsion were poured in the specimen stage, which was introduced in a cold chamber at -190°C and 10^{-4} bar room. The sample was cut to remove the first layers of emulsion. The chamber was heated up to -55°C to sublimate the water (for 2min), and then re-cooled at -190°C before starting the observation.

Granulometry was performed on a Mastersizer 3000 Static Light Scattering (SLS) equipped with red (632.8 nm) and blue (470 nm) lasers.

Optical micrographies were taken on a bright-field upright microscope (Zeiss Axioscope 40, Leitz Ortholux II) and the recorded images were analyzed with ImageJ.

The macroporosity of the samples was studied by mercury intrusion/extrusion porosimetry using a Micromeritics Autopore IV 9500 equipment (Micromeritics Corp., Norcross, GA, USA) with the following parameters: contact angle = 130°, mercury surface tension = 485 $mN \cdot m^{-1}$, maximum intrusion pressure = 224 MPa.

Pycnometry measurements were performed with a 25 mL tank filled with pure water with 0.1% of soap solution. Porous materials were immersed and weight measurement were made 5 times.

Laser Scanning Confocal Microscopy images were acquired on an inverted Leica TCS SP5 microscope equipped with an HCX PL APO 63X, NA 1.4 oil immersion objective in fluorescence mode. The laser outputs were controlled *via* the Acousto-Optical Tunable Filter (AOTF) and the collection window using the Acousto-Optical Beam Splitter (AOBS) and photomultiplicators (PMT) as follows: FITC was excited with an argon laser at 488 nm (30%) and measured with emission setting at 495-550 nm. The Helium-Neon laser at 633 nm (10%) was only used in transmission mode. Images were collected in simultaneous mode at 400 Hz with a resolution of 1024*1024 pixels.

Grafting of the ATRP Initiator on the CNC particles (synthesis of CNC-Br)

Following the protocol of Thielemans et al.,[34] 1 g of CNCs was introduced in a reaction vessel with 1 g of DMAP and 4.25 g of Bibb (reactant), 50 mL of dried DMF were then introduced under controlled atmosphere and 2.4 g of TEA were added to initiate the reaction. The reaction was performed for 1, 4 or 72 hours at 0°C, to produce nanoparticles with different esterification levels (CNC-Br_1, CNC-Br_4 and CNC-Br_{72}, respectively). The reaction was then quenched by pouring the

reaction medium in a mixture of THF and ethanol (100 mL each). After a centrifugation step (7200 g, 15 min, 15°C), the CNC-Br material was redispersed in water, and precipited in a THF/diethyl ether mixture (50/50 v/v), until the yellowish color disappeared (performed up to five times). The dispersion in water was finally freeze-dried at -52°C overnight. The grafting was confirmed through the observation of the infrared stretching vibrations of the grafted ester group at 1760 cm^{-1} (ν(C=O)) and 1060 cm^{-1} (ν(C-O)) (Figure 1). The morphology of the CNCs before and after the modification was characterized by AFM (SI, Figure S1).

Synthesis of Bis(2-pyridylmethyl)octadecylamine (BPMODA)

2-(Chloromethyl)pyridine hydrochloride (2.1 g, 12.8 mmol) was dissolved in 10 mL of water, then the pH was adjusted to 8 with a solution of NaOH at 5 mol/L. Octadecylamine (1.64 g, 6.09 mmol) was dissolved in 30 mL of DCM. The two solutions were mixed and vigorously stirred. A NaOH solution (5 mol/L) was progressively added to the mixture to maintain the pH at 8-9 for a week. The organic phase was collected, washed three times with 200 mL of distilled water, and then concentrated. The obtained product was purified by chromatography, using a neutral activated alumina oxide column, with cyclohexane/ethyl acetate (4/1, v/v) as eluent. The final product was analyzed by ^{1}H NMR (SI, Figure S2).

Yield base on gravimetric measurement = 17%.

^{1}H NMR (400 MHz, $CDCl_3$) δppm): 8.5 (d, 2H), 7.65 (t, 2H), 7.55 (d, 2H), 7.10 (t, 2H), 3.8 (s, 4H), 2.55 (t, 2H), 1.5-1.2 (m, 32H), 0.85 (t, 3H) ppm.

Grafting of the fluorescent dye on the CNC-Br particles (synthesis of FC-CNC-Br_4)

In a first step, the CNC-Br_4 particles (100 mg) were dispersed in 5 mL of dry DMF with stirring. A 5 mL DMF solution of DMAP (0.4 mmol, 48,8 mg) and Succinic anhydride (400 mg, 4 mmol) was then added and reacted for 5 hours, until the liquid turned brown. The succinylated particles were then precipited into 100 mL (0°C) of methanol and centrifugated.

Yield by gravimetry = 46 %.

In a second step, the succinylated particles (45 mg) were dispersed in 1 mL of dry DMF containing HBTU (6 mg, 0.0158 mmol). A second solution was prepared by dissolving FC (6 mg, 0.0092 mmol) and DIEA (2.4 µL, 0.0140 mmol) in a mixture of dry DMSO (120 µL) and dry DMF (47 µL). Once homogenized, this solution was added to the first one, and reaction was conducted overnight at room temperature, protected from light. The reaction was quenched by addition of 1 mL of water, and the precipited solid was dialyzed against deionized water until any trace of free FC was removed. The final dispersion was freeze-dried overnight and a yellow powder (FC-CNC-Br4) was obtained. Yield by gravimetry = 64 %.

Preparation of the emulsions

Direct emulsions:

St or *n*-BuA were mixed with $CuBr_2$, BPMODA and Ebib ([monomer]/[$CuBr_2$]/[BPMODA]/[Ebib] = 200/0.2/0.2/0.5), then gradually added (without stirring) to a water suspension containing both CNC-Br_4 and CNC-As_9 particles. The final fraction of monomer/water was fixed at 10/90 v/v and the total volume of the emulsion was 20 mL. To investigate the impact of particles concentration on the emulsion droplets, the amount of CNC-Br

was varied from 0 to 20 g/L of monomer, and that of CNC-As$_9$ from 0 to 10 g/L. The O/W emulsification was performed by sonication for 60 sec (3 sec/mL of emulsion) with a BioBlock vibra-cell equipped with an ultrasonic tip (3.0 sec on and 3.0 sec off at 30% power). NaCl (20 mM compared to the water phase) was added right after the emulsification process to avoid flocculation of the CNCs. Emulsions were allowed to rest at room temperature for 24 hours before microscopic observations and polymerizations.

Inverted emulsions:

W/O St emulsions were prepared by sonicating (3 sec/mL, 3.0 sec on and 3.0 sec off at 30% power) 3 mL of water containing 0.011 mmol of Ascorbic acid mixed with 4 mL of St (26.3 mmol) containing $CuBr_2$ (0.026 mmol), BPMODA (0.026mmol) and 40 mg of CNC-Br$_{72}$ particles. The final fraction of St/water was fixed at 57/343 v/v and the total volume of the emulsion was 7 ml. Emulsions were allowed to rest at room temperature for 24 hours before microscopic observation and polymerization.

Double emulsions:

W/O/W St emulsions were prepared by pouring the previous inverted emulsion in 13 mL of water containing 0.26 mmol of NaCl, 0.11 mmol of Ascorbic acid, 35 mg of CNC-Br$_4$ and 35 mg of CNCAs$_9$. The final fraction of styrene/water was fixed at 20/80 v/v and the total volume of the emulsion was 20 mL. The inverted emulsion in this case was made by sonication at 50% power. The double emulsification was provoked by stirring the mixture with an ultraturrax device at 8 000 rpm for one minute. The double emulsions were characterized and polymerized 1h after emulsification.

Styrene conversion = 67% by gravimetry.

Characterization of the Pickering emulsions before and after polymerization

The size of the emulsions was evaluated by measuring the Sauter Diameter ($D_{3,2}$), which corresponds to the diameter of a sphere having the same Volume/Area ratio than that of the measured object: $Sauter\ D_{3,2} = \frac{\sum f_i D_i^3}{\sum f_i D_i^2}$.[35] The Sauter diameter was either determined by granulometry, or calculated from the microscopic pictures with the help of ImageJ. The error bars were determined from the uniformity parameter (U), (calculated in the same way using the equation $U = (1 / d_{50}) \times (\Sigma \mid d_{50} - d_i \mid \times V_i) / (\Sigma V_i)$ with d_{50} the median diameter, d_i the measured diameter and V_i the volume of the sphere of d_i diameter.

The size and volume of the pores in the material produced after polymerization of the inverted emulsion, were determined by mercury porosimetry, using the following equation: $D = -4\gamma \cos(\theta) / P$ with D the diameter, γ the surface tension of mercury, θ the contact angle and P the pressure applied on the mercury.

Polymerization of the emulsions

For all experiments polymerizations were carried out in 30 mL sealed vials, under nitrogen atmosphere and without stirring.

<u>Direct emulsions with sacrificial initiator:</u>

24 hours after emulsification, 0.04 mmol of ascorbic acid (350 µL) was added and the medium was heated at 80°C. After 14 hours, the reaction was cooled at room temperature, quenched under atmosphere and characterized by optical and electronic microscopies. The polymerized beads were heated under vacuum at 80°C overnight, to remove any residual water and monomer.

For the determination of molecular masses, the dried polymer beads were dissolved in THF. The free polymer produced by the sacrificial initiator (Ebib) was separated from the CNCAs$_9$ and polymer-grafted CNC-Br$_4$ particles (St-*g*-CNC-Br$_4$ or *n*-BuA-*g*-CNC-Br$_4$) by centrifugation. The free polymer was subsequently dried (m = 10 mg) and dissolved in 1 mL of THF then analyzed by SEC. All the calculated masses are related to a polystyrene calibration.

The kinetics of polymerization were followed by ^{1}H NMR, using two different protocols depending on the monomer used. With *n*-BuA, aliquots were taken from the emulsion vials at different times and dissolved in deuterated THF. With St, the polymerization was directly performed inside a NMR tube at 80°C, with D_2O as continuous phase. The disappearance of the monomer double bond signal at 5.9-6.3 ppm for the *n*-BuA and 5.2 and 5.7 ppm for the styrene allowed us to estimate Vp.

Direct emulsions without sacrificial initiator:

The same protocol as in the previous section was used, without addition of sacrificial initiator. After 14 hours, the mixture was cooled down, opened to air and the emulsions were dried under vacuum at 70°C overnight, before being stained and characterized by Scanning Electron Microscopy. With St, a classical SEM device at room temperature was used, while the polymer produced from *n*-BuA was analyzed in its glassy state (at -190 °C), by cryo-SEM. Monomer conversions were calculated by gravimetry, after removal of any traces of monomer and water.

Inverted emulsions:

Polymerization was performed 24 hours after emulsification. During this time, the emulsion droplets sedimented. The supernatant layer composed of pure styrene was then removed and the bottom phase, containing the water droplets, the styrene continuous phase and the CNC-Br_{72} particles, was polymerized by heated the emulsion at 80°C for 14 hours. Polymerization was quenched by lowering the temperature and opening to air. The porous solid obtained was separated in two before being dried under vacuum at 70°C overnight. Half of the sample was analyzed by electronic microscopy analysis (SEM), the other half by mercury porosimetry. Since no sacrificial initiator was used for this experiment, the molecular masses could not be evaluated. Styrene conversions were calculated by gravimetry after removal of any traces of monomer and water.

Mercury porosimetry measurement were performed on the sample after vacuum drying for an additional week at 50°C under vacuum. Two mercury intrusion pressure of 0.1 and 10 MPa were found, corresponding to pores size of around 100 and 0.1 μm.

Double emulsions:

Polymerization was performed 1 hour after emulsification, by heating the mixture at 80°C for 14 hours. After reaction quenching by lowering the temperature and opening to air, the dried polymerized sample (70°C overnight) was analyzed by optical and electronic microscopies. Since no sacrificial initiator was used for this experiment, the molecular masses could not be evaluated. Styrene conversions were calculated by gravimetry after removal of the residual styrene and water.

Results and discussion

Immobilization of the ATRP Initiator on the CNC particles

In previous work, we have shown that direct O/W or inverted W/O emulsions can be efficiently stabilized by esterified CNC, provided that the hydrophilic/hydrophobic balance at particles surface is well adjusted.[6,7,36,37] This can be achieved in particular by grafting appropriate moieties and controlling the level of modification. In the current paper, an ATRP initiator was grafted at surface of the CNC by esterification with Bibb. The modified particles (CNC-Br) were used to stabilize direct or inverted monomer emulsions depending on the grafting level. The controlled AGET ATRP polymerization of these systems, initiated from the particles stabilizing the Pickering emulsion, was then investigated. This process was referred to as Pickering Emulsion Interface-Initiated Atom Transfer Radical Polymerization (PEII-AGET-ATRP). To indirectly determine the molar mass of the polymer growing from the CNC-Br particles, a sacrificial initiator (Ebib) was sometimes added in the oil phase (only for direct emulsions).

Isobutyrate bromide initiating sites were first introduced at the CNC surface, following an esterification procedure already described by Thielemans *et al* (SI, Figure S3).[34] The CNCs were reacted with Bibb for 1, 4 or 72 h (in DMF), to produce particles with various level of modification (CNC-Br_1, CNC-Br_4 and CNC-Br_{72}, respectively). The success of the reaction was first verified by observing the characteristic vibrations of the grafted Isobutyrate bromide moieties in the FTIR spectra, identified at 1760 cm^{-1} ($\nu_{(C=O)}$) and 1060 cm^{-1} ($\nu_{(C-O)}$) (Figure 1). As expected, the intensity of these vibrations increased with reaction time, while the intensity of the ν_{OH} vibrations of cellulose (at 3000-3500 cm^{-1}) concomitantly decreased. This confirmed that the reaction was efficient and time dependent. The bromine content in the modified particles was subsequently evaluated by elemental analysis and the results obtained reported in Table 1. From these data, it was also possible to estimate the rate of OH substitution at the CNCs surface (Table 1), assuming

an amount of surface OH groups of 3.10 mmol.g^{-1} for unmodified CNCs (estimation made in a former study performed with particles taken from the same batch)[32] (calculations in SI, Figure S4). The OH substitution above 100 % found for the CNC-Br_{72} sample can be explained by a slight underestimation of the OH content at the CNCs surface, due to the variability of the initial material. It is also possible that some nanocrystals were slightly damaged by the treatment in that case, although the morphology of the particles observed by AFM was not significantly modified (SI, Figure S1). In any case, the amount of initiating sites in the three modified samples can be classified as low, medium and high.

Table 1. Amount of Br sites in the esterified CNC, evaluated by elemental analysis.

Esterified Particles		**CNC-Br_1**	**CNC-Br_4**	**CNC-Br_{72}**
Brome content	wt %*	1.50	9.96	27.37
	mmol/g of cellulose	0.19	1.25	3.43
OH substitution at the CNCs surface	mol.%**	6	40	110

*Determined by elementary analysis, **Assuming a surface OH content of 3.10 mmol.g^{-1} for the unmodified CNC.[28]

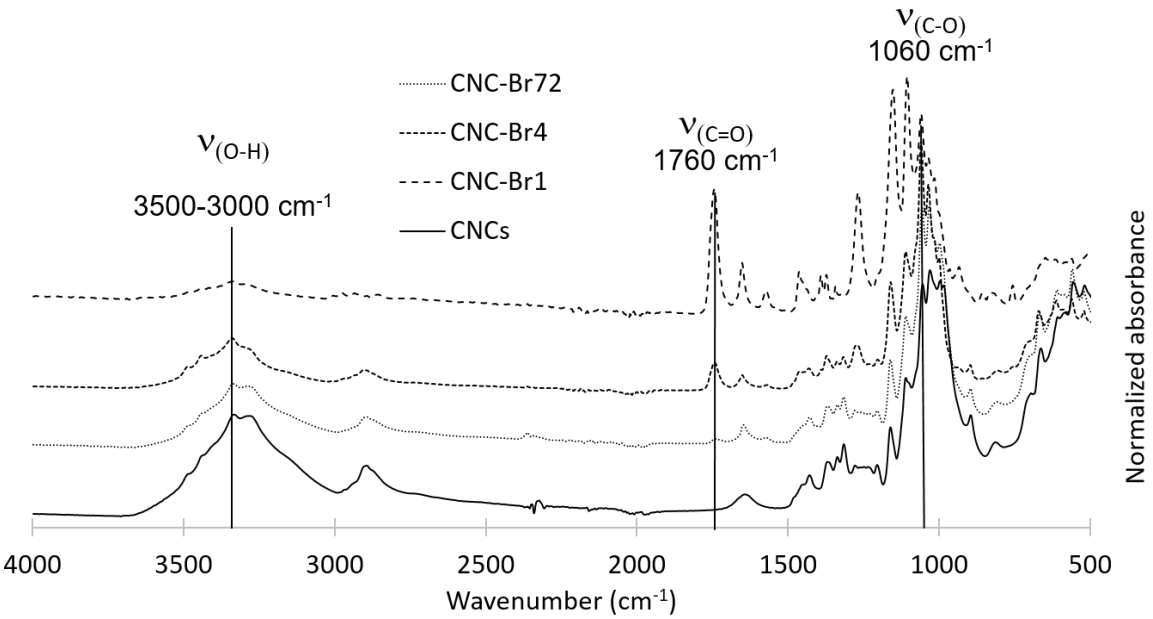

Figure 1. FT-IR spectra of the CNCs before and after esterification with Bibb.

Preparation and characterization of the Pickering Emulsions

The type of emulsion formed by the different esterified particles was first investigated, using St as monomer. In each experiment, emulsification was performed by sonicating a mixture of water, CNC-Br particles, and styrene containing the catalytic system. The particles concentration was set to 5g/L relative to the oil phase, based on results obtained in our previous investigation.[7] The CNC-Br_1 and CNC-Br_4 particles were introduced in water, but the hydrophobic CNC-Br_{72} particles required to be dispersed in the styrene phase, as they flocculated in water. The type of emulsion obtained (O/W or W/O) was inferred by observing what happened when a drop of the emulsion was added to a volume of pure styrene or pure water. Both CNC-Br_1 and CNC-Br_4 particles led to direct O/W Pickering emulsions, while the highly modified CNC-Br_{72} particles stabilized inverted W/O emulsions (Figure 2). This result is consistent with the low, medium and high hydrophobicity expected after esterification of the CNCs for 1, 4 and 72h, respectively. The type of emulsion obtained is indeed determined by the particle wettability, which is in favour of O/W emulsions

when the particles have more affinity for water, and W/O emulsions when they have more affinity for the oil phase.[38,39] Since the CNC-Br_1 particles contained a low amount of brominated initiating sites (Table 1), they were discarded in subsequent investigations.

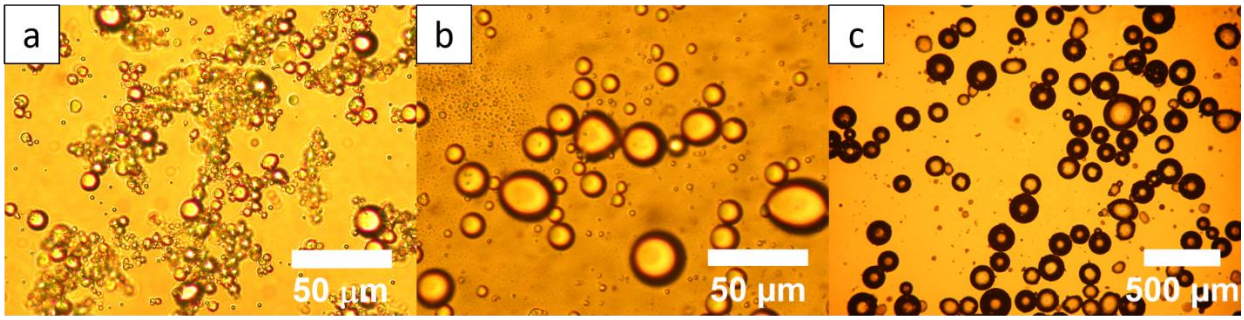

Figure 2. Optical micrographs of the direct O/W (a, b) or inverted W/O (c) St emulsions stabilized with a) CNC-Br_1, b) CNC-Br_4 and c) CNC-Br_{72} (O/W ratio =10/90 v/v; 5g CNC-Br /L of St).

Direct Emulsions

Direct O/W emulsions of St were again prepared with the CNC-Br_4 material and the impact of particles concentration on the size of the droplets was investigated. The particles were introduced in the water phase. The catalytic system introduced in the oil phase was composed of $CuBr_2$, BPMODA and Ebib. Ebib was added as a sacrificial initiator, to concurrently produce unbounded chains that will be later used to indirectly evaluate the molar mass of the grafted polymer (by SEC and ^{1}H NMR). After emulsification, NaCl (20 mM) was introduced in the system to enhance the coverage of the droplets, as CNCs (CNC-Br or CNCAs) exhibits negatively charged surface, involving repulsions, limiting the coverage at the interface, as seen in previous work.[7] Ascorbic acid – also required for the AGET ATRP polymerization – was not introduced at this stage of the study.

The average reciprocal Sauter's diameter ($1/D_{3,2}$) of the emulsions increased linearly with the particles concentration between 0 and 5 g/L of St (Figure 3), in agreement with the limited

coalescence mechanism.[40] When the CNC-Br_4 concentration was further increased, the amount of particles exceeds the amount needed to cover the created interfacial area. Hence the O/W interface created during sonication was quickly stabilized (the neighboring droplets did not coalesce anymore) and the average size of the droplets remained constant, while a broad polydispersity was now measured, as a result of the polydispersity directly resulting from the emulsification process. In view of these results, a concentration of 5 g CNC-Br_4/L of St was selected in further investigations, as it allowed maximizing the number of initiating sites at the surface of the droplets (high surface area), while maintaining a quite narrow dispersity.

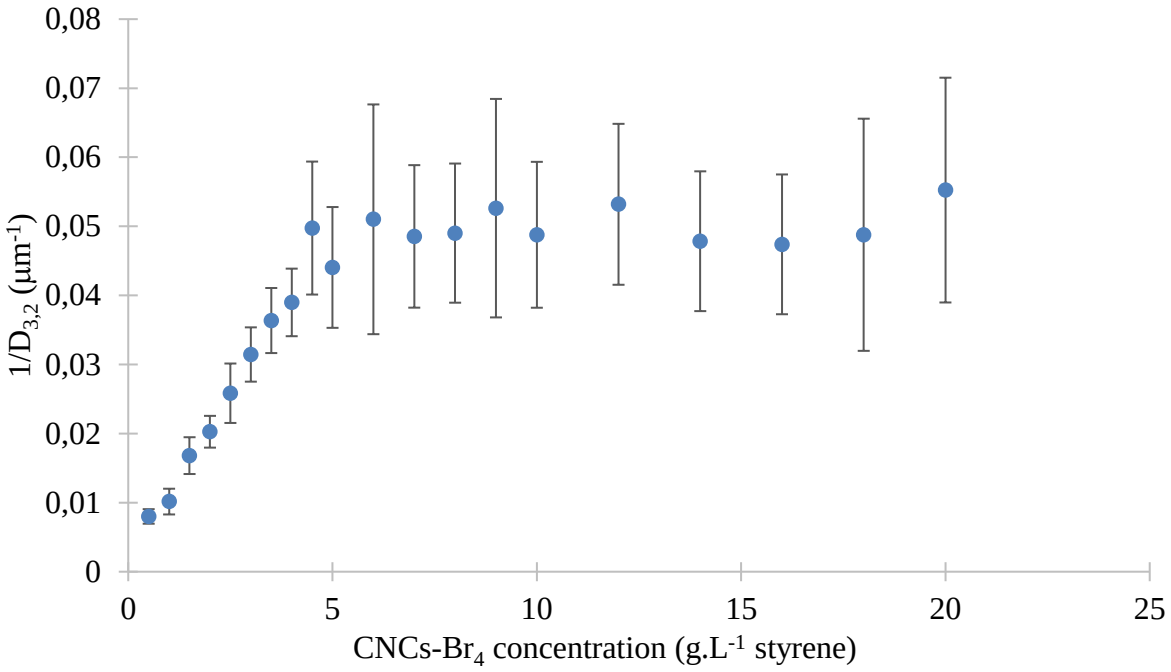

Figure 3. Evolution of the reciprocal Sauter's diameter of the O/W St emulsion droplets as a function of CNC-Br_4 concentration (O/W ratio =10/90 v/v). The error bars represent the emulsion polydispersity.

The stability of the St O/W emulsions (5 g CNC-Br_4/L of St) were further investigated by observing the evolution of the droplets size and morphology after i) one-month storage at 6°C, and

ii) 14 hours heating at 80°C, temperature later used to initiate the polymerization (no polymerization occurred at this stage, since Ascorbic acid was not yet introduced in the system). No phase separation occurred after one month at 6°C, although the size and form of the droplets changed slightly (SI, Figure S5). A neat phase separation was however observed after the heating step at 80 °C. To circumvent this problem, acetylated CNCs ($CNCAs_9$) were added before emulsification, as these particles already proved their efficiency to stabilize the styrene emulsions under heat.[7] A new set of experiment was therefore performed, using various concentrations of $CNCAs_9$ and $CNC\text{-}Br_4$ particles. The size of the Pickering emulsions droplets obtained 24 hours after emulsification (at room temperature), is compared in Table 2. The introduction of the $CNCAs_9$ particles in the system led to a significant decrease in droplets size, regardless of the concentration in $CNC\text{-}Br_4$ particles. Since 5g $CNCAs_9$/L of St were sufficient to obtain quite small droplets (~ 8 μm), a mixture of 5g/L $CNC\text{-}Br_4$ + 5g/L $CNCAs_9$ was selected in subsequent investigations.

Table 2. Size of the O/W St emulsions obtained (in μm) after sonication with various concentrations of $CNCAs_9$ and $CNC\text{-}Br_4$ Pickering Particles. Measurements were performed by granulometry, 24 hours after emulsification at room temperature.

$CNCAs_9$ g/L \ **$CNC\text{-}Br_4$ g/L**	**0**	**2**	**5**	**10**
0	demixion	49.4 ± 5.6	22.7 ± 4.5	20.5 ± 4.4
2	12.4 ± 2.4	13.3 ± 2.9	11.1 ± 2.2	13.0 ± 2.8
5	10.0 ± 2.8	9.6 ± 3.1	7.8 ± 1.5	8.9 ± 1.9

10	11.3 ± 2.6	9.0 ± 2.5	7.3 ± 1.4	10.5 ± 6.3

Inverted and double emulsions

Inverted W/O emulsions of St were prepared with the hydrophobic CNC-Br_{72} particles, this time introduced in the oil phase containing $CuBr_2$, BPMODA and Ascorbic acid. The average reciprocal Sauter's diameter ($1/D_{3,2}$) of the emulsions increased with the concentration, exhibiting an unexpected behavior (Figure 4). The droplet population between 2 and 5 $g.L^{-1}$ do not increased in diameter, which can be explained by the formation of a smaller population of droplet, located inside the droplet of water, partitioning the CNC-Br_{72} between the two populations (Figure 5, a and b). These small droplets are probably composed of styrene which is why they tend to aggregate at the top of each water droplet ($d_{st} < d_{water}$)(Figure 5, a, b and c). By increasing further the CNC-Br_{72} concentration, the size of these droplets decreased, until they could be only observed by SEM above 5 $g.L^{-1}$ (Figure 5, c, d, and Figure 12 c). Then, $1/D_{3,2}$ increased linearly with the particles concentration as expected, in line with the limited coalescence mechanism. The end of the limited coalescence was not attained, because higher concentrations of CNC-Br_{72} could not be dispersed in the styrene phase. In view of these results, a CNC-Br_{72} concentration of 10 $g.L^{-1}$ of St was selected in further investigations, as it represents a good compromise between size, stability and amount of initiating particles.

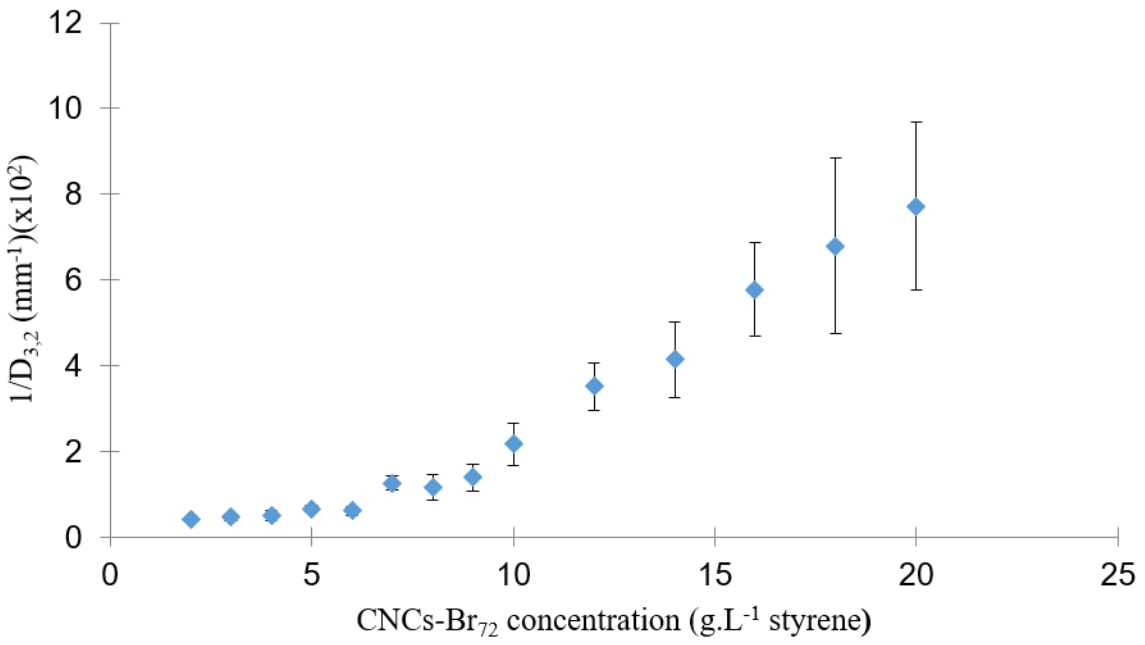

Figure 4. Evolution of the reciprocal Sauter's diameter of the W/O emulsion droplets as a function of CNC-Br_{72} concentration (W/O ratio = 57/43 v/v).

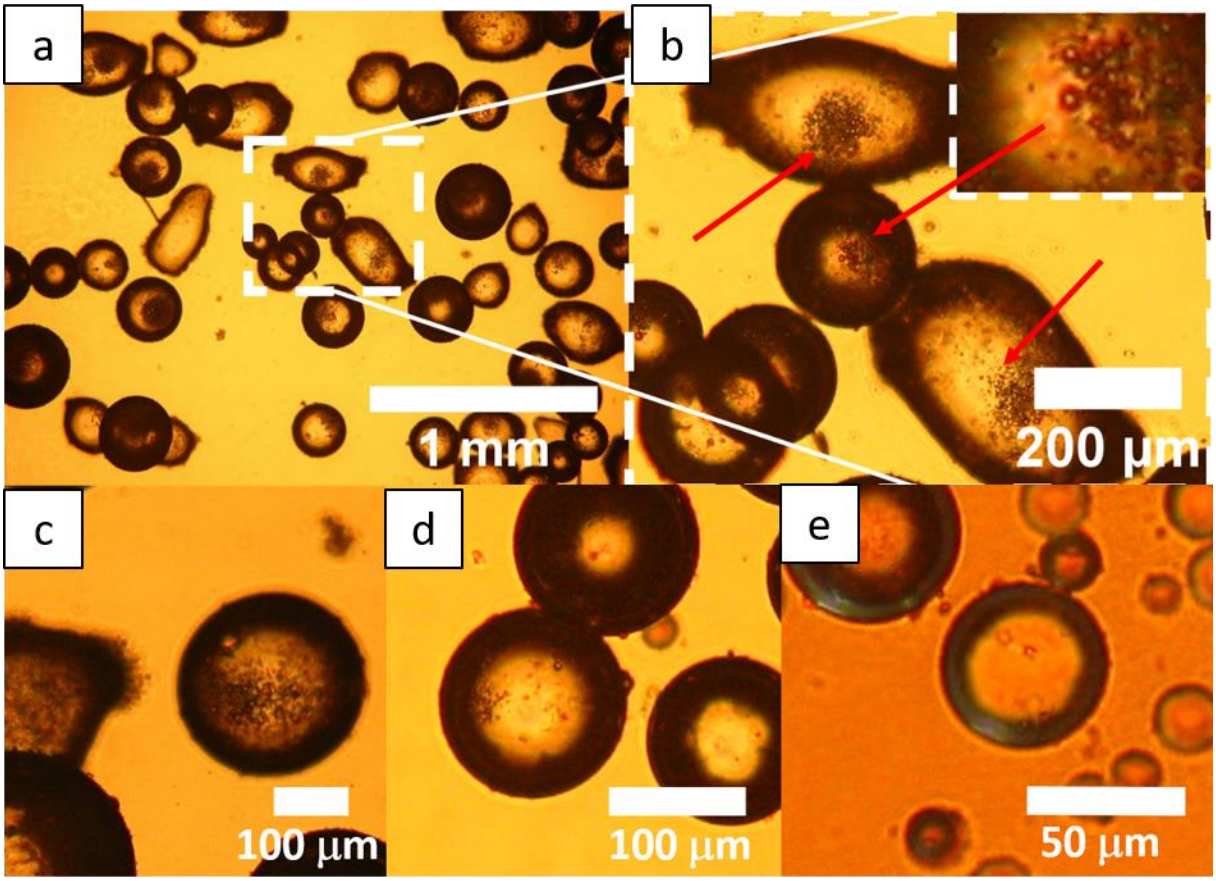

Figure 5. Optical micrographs of the invert W/O stabilized by (a, b, c) 2 $g.L^{-1}$ (d) 5 $g.L^{-1}$ and (e) 12 $g.L^{-1}$ of $CNC\text{-}Br_{72}$.

The inverted St emulsion was later poured in a water phase containing NaCl, Ascorbic acid and a mixture of $CNC\text{-}Br_4$ (5g/L) and $CNCAs_9$ (5g/L) particles, to prepare double W/O/W emulsions (see experimental section). The double emulsions were composed of micrometric globules (73 ± 33 µm in size) containing several water droplets of smaller size (21 ± 12 µm) (Figure 6). The emulsion was still stable after 48 hours, but the inner droplets progressively coalesced and escaped from the St droplets. After one month, only distorted globules remained showing the low stability of the double emulsion at this time scale.

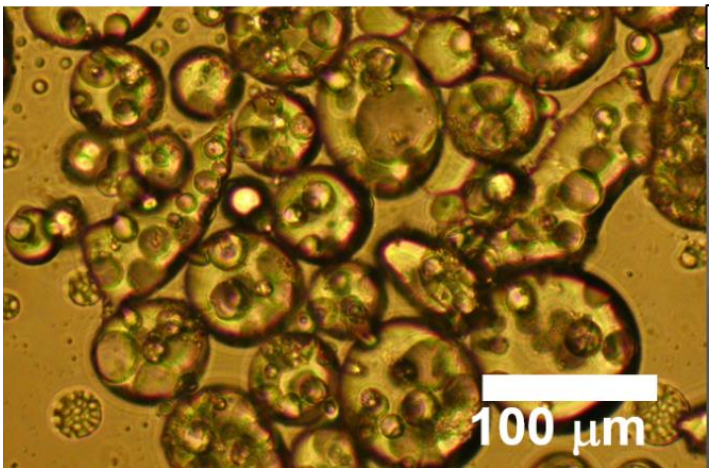

Figure 6. Images of the double W/O/W St emulsion before polymerization

Interface-Initiated Atom Transfer Radical Polymerization of the Pickering Emulsions (PEII-AGET-ATRP)

ATRP is a powerful living radical polymerization method to grow polymer brushes from nanoparticles such as the CNCs. However, it is highly sensitive to oxygen, which cannot be totally suppressed in our case, due to the sonication step. To overcome this problem, the alternative Activator Generation by Electron Transfer method (AGET ATRP) was used in the current study.

Polymerization of direct Emulsions

Direct O/W emulsions of St and *n*-BuA were prepared following the previous procedure, but this time, including ascorbic acid in the catalytic system. Ascorbic acid serves as activator in the process, by provoking the reduction of $CuBr_2$ in CuBr and therefore generating the active Cu(I) species required for the PEII-AGET-ATRP reaction. The concentration of Ascorbic acid was 10 times higher than in conventional emulsion polymerization,[29,41,42] due to the larger size (i.e. lower

specific surface area) of our Pickering emulsion droplets. The PEII-AGET-ATRP polymerization started when the emulsion was heated at 80 °C. The reaction was confined inside the stabilized droplets, as the monomers were not soluble in water.

The polymerized material obtained was composed of distorted polymer microbeads of 4 to 10 µm for polystyrene (PSt) and 10 to 20 µm for polybutylacrylate (PBuA) (Figure 7). No coagulum was detected in the medium, although some flocculated beads were observed.

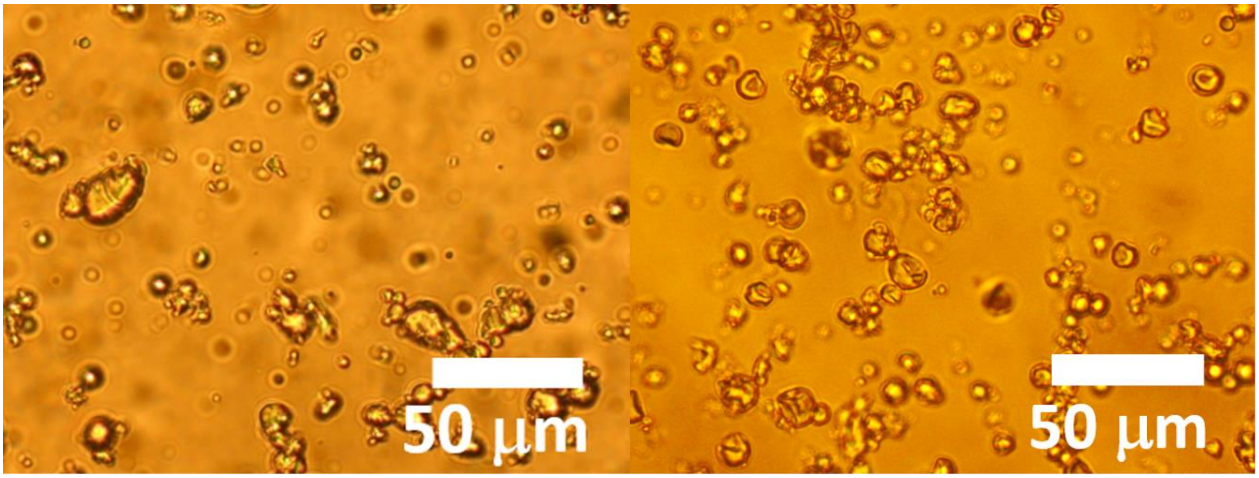

Figure 7. Optical micrographs of the beads obtained right after polymerization of the Styrene (left) and *n*-BuA (right) direct emulsions.

The monomer conversions with time were followed by ^{1}H NMR (Figure 8). In both cases, the conversion profile was linear with time, allowing a graphical estimation of the polymerization speed (Vp). Reactions were quenched after 14 hours, and the final monomer conversions were determined by gravimetry. After 3 hours, 76% of the *n*-BuA was polymerized (and the reaction did not progress anymore), while the St conversion progressed slowly, and hardly reach 24% after 14 hours. This difference in kinetics between the two monomers is not surprising, as it is well established that acrylate monomers are more reactive than styrene by ATRP.[43]

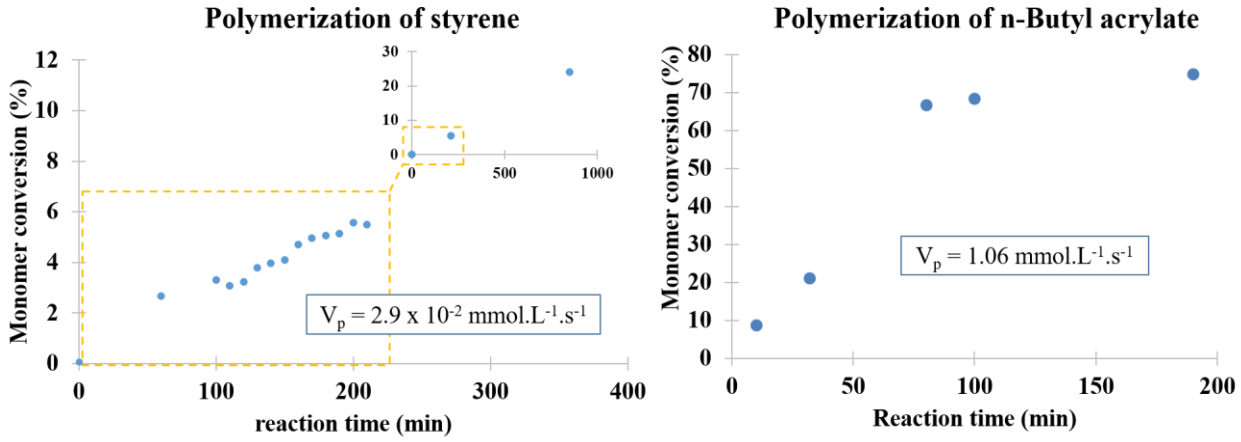

Figure 8. Kinetics of the PEII-AGET-ATRP polymerization of styrene (left) and *n*-butyl acrylate (right), followed by ^{1}H NMR.

Table 3. Experimental and theoretical average molecular masses and polydispersity index of the polymer chains evaluated by SEC analysis of the free polymer produced by the sacrificial initiator.

	$\bar{M}_n$ exp[a] g.mol^{-1}	$\bar{M}_n$ theo[b] g.mol^{-1}	M_w g.mol^{-1}	Đ
PSt	43 000	4 284	93 000	2.17
PBuA	31 800	16 008	48 700	1.53

[a] calibration with PS standard. [b] $\bar{M}_n$ theo = Conversion x M_0 x [monomer]/[initiator]

The molecular masses of the grafted polymers were indirectly determined by SEC, after analysis of the free polymers produced by the sacrificial initiator (PSt and PBuA), which was recovered after solubilization in THF and centrifugation (operation done 3 times). The values obtained ($\bar{M}_n$ exp and Đ in Table 3) were much higher than those theoretically expected after polymerization by

ATRP ($\overline{M}_n$ theo in Table 3), indicating that the higher ascorbic acid content used in our process had significant impact on the reaction. It has indeed been described in the literature that a fast initial kinetic polymerization occurs in this case, lowering the overall control of the polymerization.[42] In addition, the orientation towards aqueous phase of some grafted initiator, reduces their chance of initiating the polymerization.

The solid material remaining after the THF extraction (CNC-g-PSt and CNC-g-PBA), as well as the free polymers (PSt and PBuA), were separately analyzed by FT-IR spectroscopy (Figure 9). The FT-IR signatures of the cellulose nanocrystals and synthesized polymers are both detected in the spectra of the extracted solid samples, confirming that the ATRP reaction also initiated from the bromoisobutyrate sites at the CNC surface, leading to the expected CNC-g-PSt and CNC-g-PBuA hybrid materials. In both spectra, cellulose is, as seen before, particularly apparent at 3050-3500 cm^{-1} (ν_{O-H}) and 900-1400 cm^{-1} (ν_{C-O}, ν_{C-C}, δ_{O-H}, δ_{C-H}), while the PSt can be seen at 1600, 1500 and 1450 cm^{-1} in CNC-g-PSt ($\nu_{C=C}$ of the aromatic rings), and the PBuA at 1750 ($\nu_{C=O}$) and 1050-1300 cm^{-1} (ν_{C-O}) in CNC-g-PBuA.

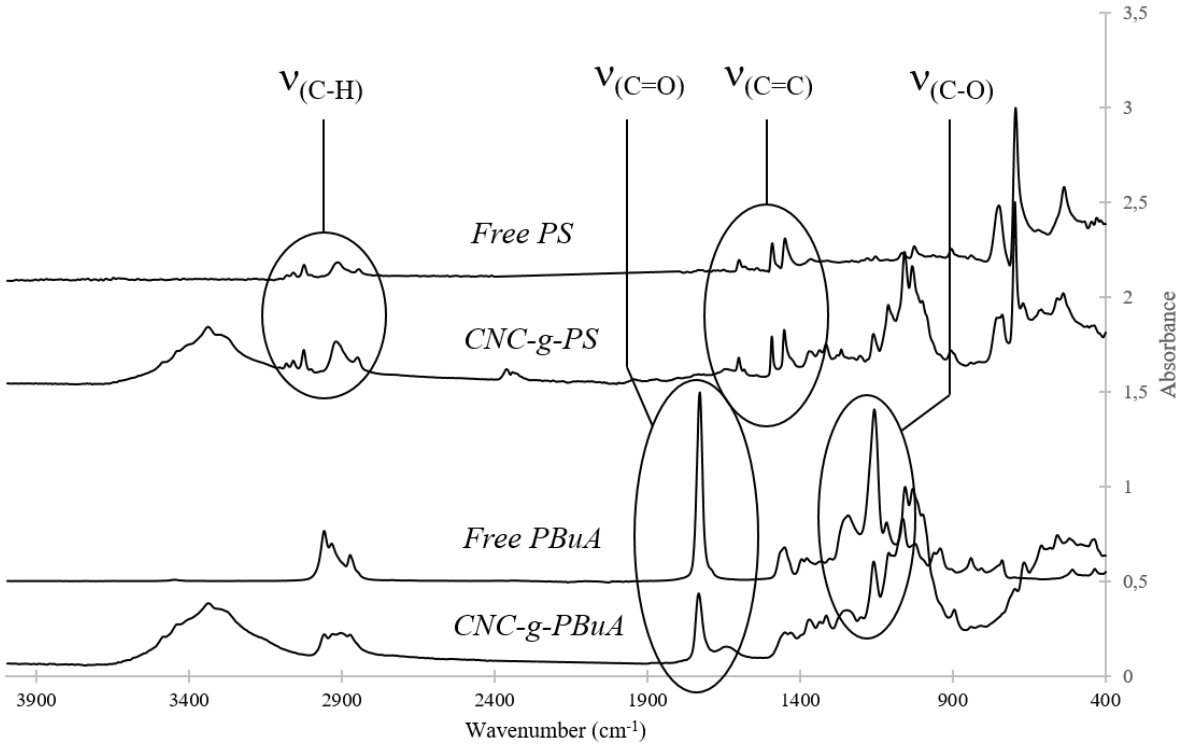

Figure 9. FT-IR spectra of the solid material remaining after the THF extraction (CNC-g-PSt and CNC-g-PBuA), and free polymers recovered (PSt and PBuA) after elimination of the solvent.

The PEII-AGET-ATRP polymerization of the St and *n*-BuA emulsions was performed again in the same conditions, but this time without the sacrificial initiator. The PSt beads obtained were analyzed by classical scanning electron microscopy (SEM) at room temperature (Figure 10), while the PBuA beads were analyzed by cryo-SEM at -190°C, to remain below its glassy state (T_g PBuA = -49°C; SI, Figure S6).

Two different morphologies were apparently obtained depending on the polymer. Indeed, empty capsules were spotted in the SEM micrographs with PSt (pointed by the dashed arrow in Figure 10b), while plain beads were mostly seen in the case of PBuA (plain arrow in Figure 10c). This result is not surprising in view of the monomers conversions measured in Figure 8. Due to the low conversion of the styrene monomer (yield = 18 %), only the volume close to the shell could be

polymerized, leading to the capsules observed in Figure 10b. On the other end, the higher conversion obtained with the *n*-BuA monomer (yield = 66 %) allowed the polymerization of a higher volume, leading to the filled beads observed in Figure 10c,d. Therefore, by simply controlling the monomer conversion, it should be possible to tune the morphology of the polymerized spheres (empty or filled), which is a clear advantage compared with the reported method, where the initiator is not bound to the particles stabilizing the Pickering emulsions.[7]

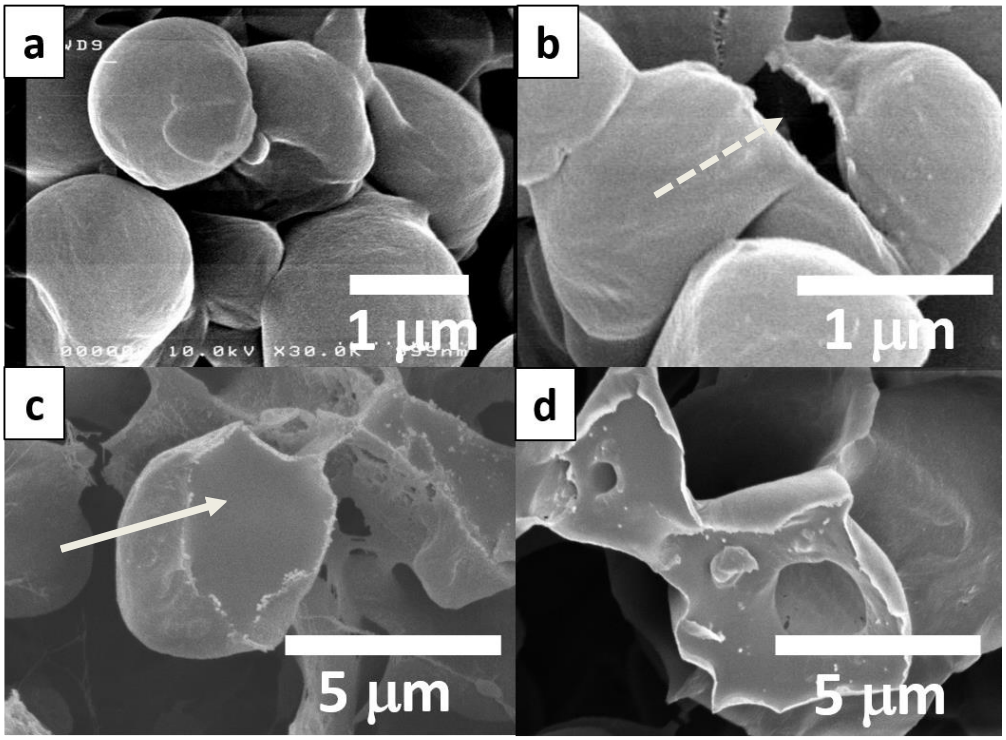

Figure 10. SEM micrographs of the PSt beads (a, b) and cryo-fractured PBuA beads (c, d) obtained after PEII-AGET-ATRP polymerization of the emulsions, performed without sacrificial initiator. The dashed arrow points at an empty CNC-g-PSt capsule; the plain arrow points at a plain CNC-g-PBuA bead (cut in half by cryo-fracture).

It can be noted that, in the case of the PBuA polymer, the molecular mass measured by SEC ($\overline{M}_n$ = 31 800 g.mol^{-1}) suggests that the chains at the center of the beads are not bonded to the CNC-

shell since the beads are micrometric. A likely hypothesis would be that some free CNC-Br_4 migrated to the inner phase, where they initiated some polymerizations. To verify this point, a fluorescent molecule was grafted at the surface of the CNC-Br_4 particles (FC-CNC-Br_4), following a protocol reported in the literature.[44] A new O/W emulsion of *n*-BuA was then prepared, with 5 $g.L^{-1}$ of FC-CNC-Br_4 and 5 $g.L^{-1}$ of $CNCAs_9$. This emulsion was analyzed before and after polymerization, by laser confocal fluorescence microscopy (Figure 11). Before polymerization, the FC-CNC-Br_4 particles are only located at the O/W interface of the *n*-BuA droplets. During and after polymerization on the other hand, many FC-CNC-Br_4 particles are spotted inside the polymerizing droplets or final PBuA beads (green color).

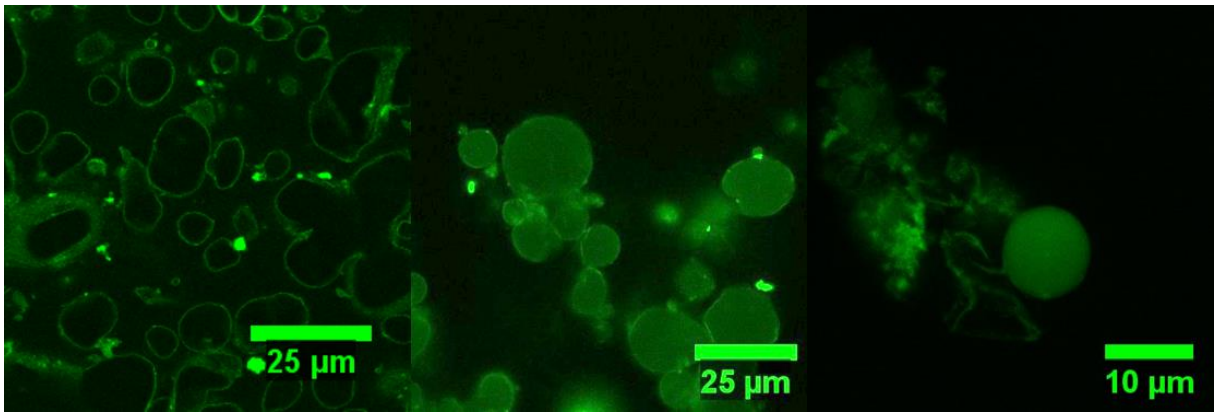

Figure 11. Laser confocal fluorescence microscopy of the O/W *n*-BuA emulsion stabilized by the FC-CNC-Br_4 particles, before (left), during (center) and after (right) polymerization (O/W ratio: 1/9 v/v; 5g/L FC-CNC-Br_4, 5g/L $CNCAs_9$).

The migration of part of the FC-CNC-Br_4 particles during polymerization was assigned to the increasing hydrophobicity of their surface, imparted by the growing PBuA chains. Some of the CNC-g-PBuA particles probably desorbed from the interface during the process, and migrated towards the center of the oil phase, where polymerization continued.

Polymerization of inverted Emulsions

The inverted W/O St emulsions prepared with the hydrophobic CNC-Br_{72} particles were polymerized by heating the mixture at 80°C for 14 hours. The greenish solid obtained was subsequently dried under vacuum and analyzed by SEM (Figure 12). Contrary to the results obtained with the direct emulsion (24% conversion), a full conversion (100%) of the styrene was now reached after 14 hours, based on gravimetric measurement. This result can be easily explained by the higher concentration of Bromoisobutyrate sites immobilized at the surface of the CNC-Br_{72} particles (three times higher than for the CNC-Br_4 particles used in direct emulsions), which obviously initiated more polymerizations. As expected, the PEII-AGET-ATRP reaction occurred only in the external phase (St is insoluble in water), leading to the porous structure observed in Figure 12.

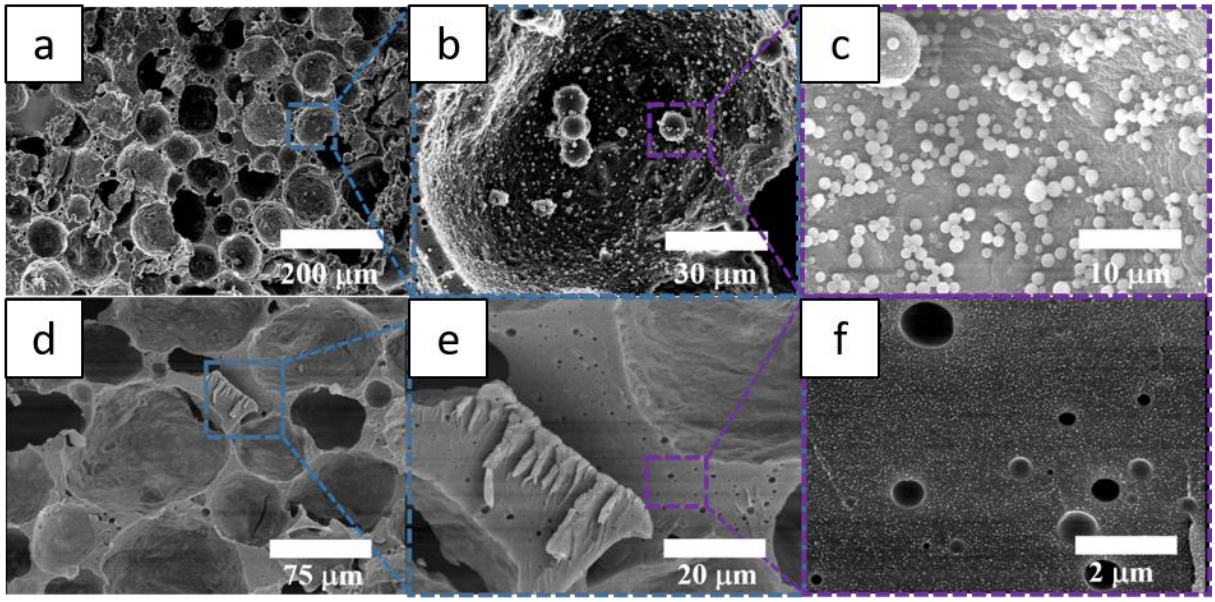

Figure 12. SEM micrographs of the PSt material obtained after PEII-AGET-ATRP polymerization of the inverted W/O St emulsion stabilized by the CNC-Br_{72} particles. The macroporosity M_1 (a

and d), macroporosity (M_2) (e and f) and small microbeads covering the surface of the macropores M_1 (b and c) are illustrated by the different magnifications.

Surprisingly, pore of different sizes, some with sizes of some micrometers (M_1) and some others with a size in the nanometer range (M_2) were observed in the SEM pictures. Whereas the formation of closely packed pores with sizes in the micrometer scale (estimated size = 76 ± 19 µm) was easily attributed to the former water droplets, the presence of pores of nanometer size in the polymerized external phase (estimated size < 1 µm) could not been explained at this stage of the study. Small microbeads were also spotted inside the M_1 pores (Figure 12 b, c), confirming that the small droplets observed inside the water phase of the W/O emulsions (see section on the characterization of the inverted emulsions) were composed of styrene, which polymerized after the heating treatment.

The porosity and density of the material were further investigated by mercury porosimetry, which confirmed the bimodal distribution of the pores size (Figure 13).

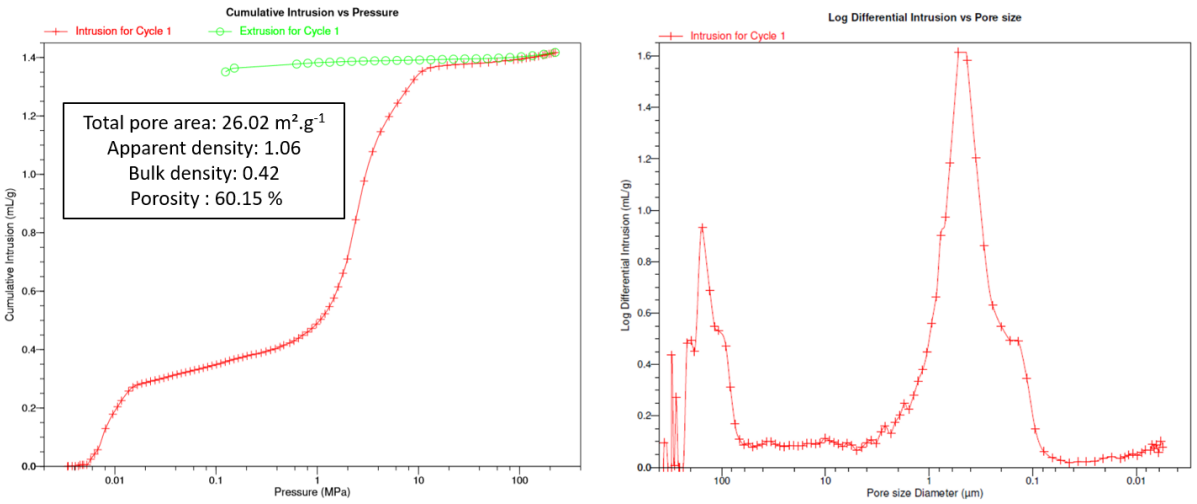

Figure 13. Cumulative intrusion (expressed as cumulative intrusion vs applied pressure) (left) and pore size distribution (expressed as Log differential Intrusion vs pore size) (right) in the polymerized inverted W/O St emulsion measured by mercury porosimetry.

The calculated skeletal density of the sample is 1.06, which agrees with the density expected for PS. Therefore, all the holes inside the material were filled by the mercury during the measurement, indicating that the pores were interconnected.

Two population could be seen: the first one, observed at 0.01 MPa, correspond to a size of 80-200 μm which is in agreement with what could be seen in SEM, at the surface of the sample (M_1 pores). The second one, much higher in intrusion value, between 2 and 20 MPa, correspond to a size of 100-1000 nm. This population was assigned first to the M_2 pores, seen in SEM, and also to M_1 pores connected by pores (or channels) of the size of M_2, which explained why the intrusion value is so high.

The total porosity was estimated at 60.15 %, with an apparent bulk density of 0.42, which tend to be overestimated in mercury porosimetry. Indeed, the real density was later confirmed to be 0.335 ± 0.012, by pycnometry.

Polymerization of double emulsions

The double W/O/W emulsion prepared with styrene was polymerized by heating the mixture at 80°C for 14 hours. Ascorbic acid was introduced in both the external and internal water phases, to increase the copper reduction yield and optimize the styrene conversion. The latex obtained after reaction sedimented quickly (because of the density of polystyrene), but could be easily

redispersed by manual shaking, as no large coagulum were detected at this stage of the study. A styrene conversion of 67% was estimated by gravimetry after emulsion drying. The analysis of the solid by SEM revealed that the latex was composed of capsules, with an estimated diameter of 50 μm and shell thickness of about 1.4 μm (Figure 14).

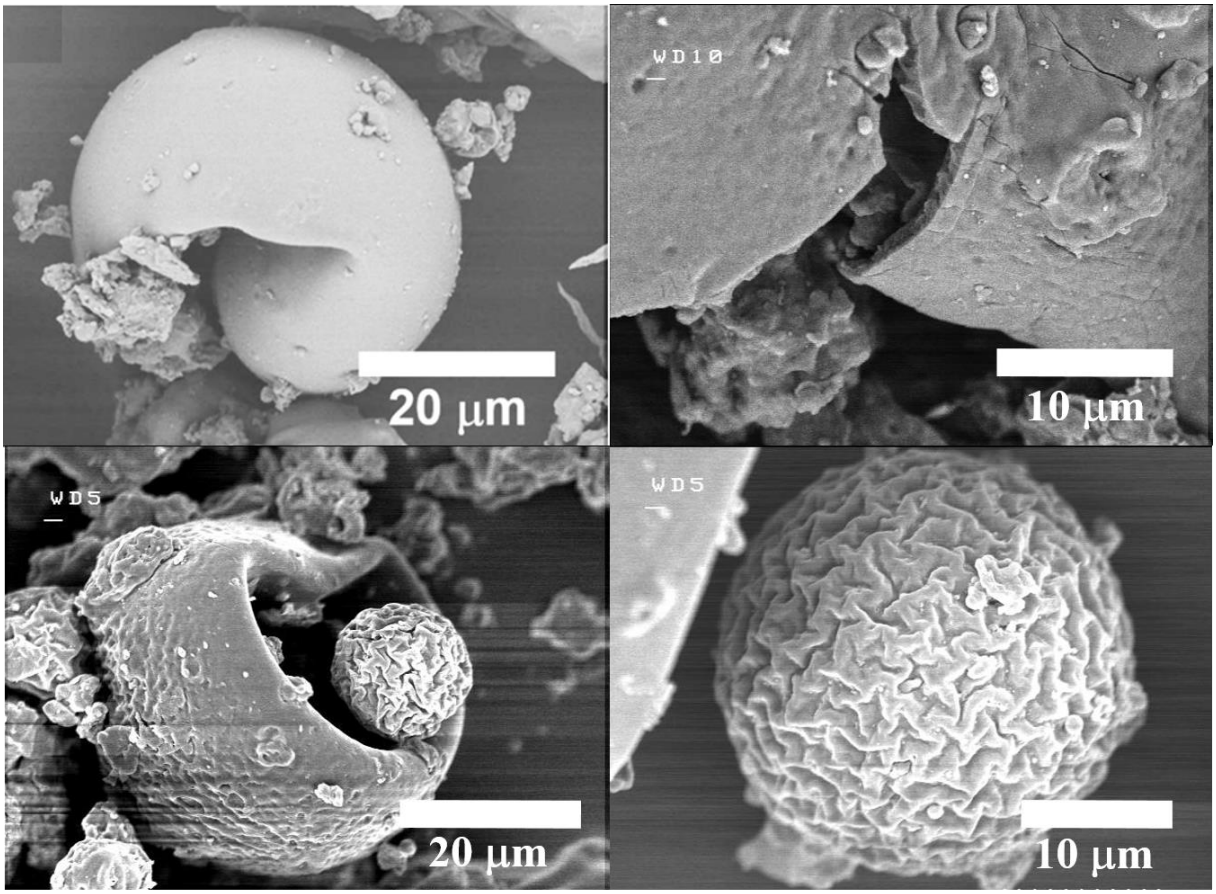

Figure 14. SEM micrographs of the PSt material obtained after PEII-AGET-ATRP polymerization of the multiple W/O/W St emulsion stabilized by CNC-Br_{72}, $CNCAs_9$ and CNC-Br_4 particles. Capsules and inner polymerized beads with PSt coagula can be seen.

The observation of some fractured capsules allowed identifying smaller beads (of about 10 μm in size), which were initially encapsulated inside the material (Figure 14). This result can be easily explained if we consider that the initiating particles (CNC-Br_{72} and CNC-Br_4) were adsorbed at

both the W/O and O/W interphases in the W/O/W emulsion (Figure 15). With this structure, polymerization can initiate both around the oil and water droplets, leading to the encapsulated (empty) beads observed in Figure 14. Surprisingly, these beads displayed an unusual "brain convolutions" aspect, with no equivalence in the literature for similar polymerization systems. This result can be explained by the fact that the PSt chains tend to grow outward, inside the styrene phase. Hence, the small empty beads have no reason to exhibit a smooth surface, since there is no difference in surface tension between the growing PSt and the surrounding St. The SEM micrographs reveal some small non-spherical objects probably resulting from a lack of droplets stability under the polymerization conditions, which mean that the stability of the former W/O/W emulsion still needs to be improved.

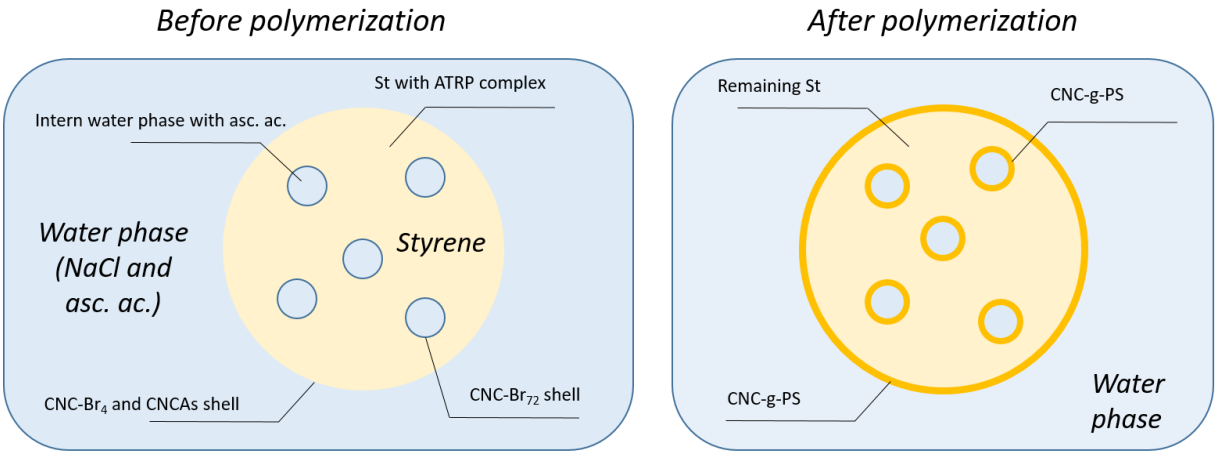

Figure 15. Schematic representation of the W/O/W emulsion before and after the PEII-AGET-ATRP polymerization.

Conclusion

We have developed a novel method to prepare capsules, beads or open-cell materials from Pickering emulsions of monomers stabilized by cellulose nanocrystals (CNCs) grafted with reactive Isobutyrate bromide moieties. The control of the grafting level at the CNCs surface allowed producing particles of medium or high hydrophobicity, which could be later used to efficiently stabilize direct (O/W) or inverted (W/O) Pickering emulsions of monomers, respectively. Double W/O/W Pickering emulsions were also prepared, by combining the two types of particles, and kept stable during more than 48h. The different emulsions obtained were subsequently polymerized, by initiating an AGET-ATRP reaction from the brominated particles surrounding the stabilized droplets. The polymerization of the direct emulsions allowed producing either capsules or filled beads, depending on the monomer used (St or *n*-BuA), which we assigned to differences in monomer reactivity. Hence, the method offers the opportunity to tune the morphology of the polymerized spheres (empty or filled), by simply controlling the monomer conversion. This is a clear advantage compared with the reported methods, where the initiator is not bound to the Pickering particles. The polymerization of the inverted emulsion on the other end, led to the formation of a porous material, with both M_1 and M_2. This type of material could easily have application as chock absorbents, thermal or sound insulators, support for catalysis… The polymerization of the double W/O/W emulsions was also envisaged, but a small amount of coagulate was concomitantly produced in that case, due to the lacking stability of the emulsion under polymerization conditions. Despite this problem, small empty beads encapsulated into larger capsules could be produced. Additional investigations are still required, but the method opens the route for the preparation of a wide range of novel polymeric materials, with original morphologies.

ASSOCIATED CONTENT

Supporting Information 1. Show the height images of CNCs and CNC-Br_{72} in AFM with the calculated length of the crystals.

Supporting Information 2. ^{1}H NMR of BPMODA with attributed signals.

Supporting Information 3. Reaction between the cellulose and the bromoisobutyryl bromide

Supporting Information 4. Information about the way to calculate the TSS.

Supporting Information 5. Direct emulsion of *n*-BuA right after emulsification and after 1 month at 6°C.

Supporting Information 6. DSC of PBuA showing the glass transition of the polymer.

Acknowledgements

We would like to acknowledge the University of Bordeaux for their fundings, Armand Roucher for his expertise with SEM device, Gilles Pecastaing for his knowledge in AFM field, PLACAMAT for the cryo-SEM experiences and Marie Anne Dourges for her expertise in mercury porosimetry.

Funding Sources

University of Bordeaux

REFERENCES

(1) Foster, E. J.; Moon, R. J.; Agarwal, U. P.; Bortner, M. J.; Bras, J.; Camarero-Espinosa, S.; Chan, K. J.; Clift, M. J. D.; Cranston, E. D.; Eichhorn, S. J.; et al. Current Characterization Methods for Cellulose Nanomaterials. *Chem. Soc. Rev.* **2018**, *47* (8), 2609–2679. https://doi.org/10.1039/C6CS00895J.

(2) Habibi, Y.; Lucia, L. A.; Rojas, O. J. Cellulose Nanocrystals: Chemistry, Self-Assembly, and Applications. *Chem. Rev.* **2010**, *110* (6), 3479–3500. https://doi.org/10.1021/cr900339w.

(3) Azizi Samir, M. A. S.; Alloin, F.; Dufresne, A. Review of Recent Research into Cellulosic Whiskers, Their Properties and Their Application in Nanocomposite Field. *Biomacromolecules* **2005**, *6* (2), 612–626. https://doi.org/10.1021/bm0493685.

(4) Lin, N.; Dufresne, A. Surface Chemistry, Morphological Analysis and Properties of Cellulose Nanocrystals with Gradiented Sulfation Degrees. *Nanoscale* **2014**, *6* (10), 5384–5393. https://doi.org/10.1039/C3NR06761K.

(5) Capron, I.; Cathala, B. Surfactant-Free High Internal Phase Emulsions Stabilized by Cellulose Nanocrystals. *Biomacromolecules* **2013**, *14* (2), 291–296. https://doi.org/10.1021/bm301871k.

(6) Sèbe, G.; Ham-Pichavant, F.; Pecastaings, G. Dispersibility and Emulsion-Stabilizing Effect of Cellulose Nanowhiskers Esterified by Vinyl Acetate and Vinyl Cinnamate. *Biomacromolecules* **2013**, *14* (8), 2937–2944. https://doi.org/10.1021/bm400854n.

(7) Werner, A.; Schmitt, V.; Sèbe, G.; Héroguez, V. Synthesis of Surfactant-Free Micro- and Nanolatexes from Pickering Emulsions Stabilized by Acetylated Cellulose Nanocrystals. *Polym. Chem.* **2017**, *8* (39), 6064–6072. https://doi.org/10.1039/C7PY01203A.

(8) Miao, C.; Tayebi, M.; Hamad, W. Y. Investigation of the Formation Mechanisms in High Internal Phase Pickering Emulsions Stabilized by Cellulose Nanocrystals. *Phil Trans R Soc A* **2018**, *376* (2112). https://doi.org/10.1098/rsta.2017.0039.

(9) Binks, B. P. Particles as Surfactants—similarities and Differences. *Curr. Opin. Colloid Interface Sci.* **2002**, *7* (1–2), 21–41. https://doi.org/10.1016/S1359-0294(02)00008-0.

(10) Zhai, X.; Lin, D.; Liu, D.; Yang, X. Emulsions Stabilized by Nanofibers from Bacterial Cellulose: New Potential Food-Grade Pickering Emulsions. *Food Res. Int.* **2018**, *103*, 12–20. https://doi.org/10.1016/j.foodres.2017.10.030.

(11) Hedjazi, S.; Razavi, S. H. A Comparison of Canthaxanthine Pickering Emulsions, Stabilized with Cellulose Nanocrystals of Different Origins. *Int. J. Biol. Macromol.* **2018**, *106*, 489–497. https://doi.org/10.1016/j.ijbiomac.2017.08.030.

(12) Kalashnikova, I.; Bizot, H.; Bertoncini, P.; Cathala, B.; Capron, I. Cellulosic Nanorods of Various Aspect Ratios for Oil in Water Pickering Emulsions. *Soft Matter* **2013**, *9* (3), 952–959. https://doi.org/10.1039/C2SM26472B.

(13) Wen, C.; Yuan, Q.; Liang, H.; Vriesekoop, F. Preparation and Stabilization of D-Limonene Pickering Emulsions by Cellulose Nanocrystals. *Carbohydr. Polym.* **2014**, *112*, 695–700. https://doi.org/10.1016/j.carbpol.2014.06.051.

(14) Kasiri, N.; Fathi, M. Production of Cellulose Nanocrystals from Pistachio Shells and Their Application for Stabilizing Pickering Emulsions. *Int. J. Biol. Macromol.* **2018**, *106*, 1023–1031. https://doi.org/10.1016/j.ijbiomac.2017.08.112.

(15) Glasing, J.; G. Jessop, P.; Champagne, P.; F. Cunningham, M. Graft-Modified Cellulose Nanocrystals as CO_2 -Switchable Pickering Emulsifiers. *Polym. Chem.* **2018**, *9* (28), 3864–3872. https://doi.org/10.1039/C8PY00417J.
(16) Saidane, D.; Perrin, E.; Cherhal, F.; Guellec, F.; Capron, I. Some Modification of Cellulose Nanocrystals for Functional Pickering Emulsions. *Phil Trans R Soc A* **2016**, *374* (2072), 20150139. https://doi.org/10.1098/rsta.2015.0139.
(17) Hu, Z.; Ballinger, S.; Pelton, R.; Cranston, E. D. Surfactant-Enhanced Cellulose Nanocrystal Pickering Emulsions. *J. Colloid Interface Sci.* **2015**, *439*, 139–148. https://doi.org/10.1016/j.jcis.2014.10.034.
(18) Cunha, A. G.; Mougel, J.-B.; Cathala, B.; Berglund, L. A.; Capron, I. Preparation of Double Pickering Emulsions Stabilized by Chemically Tailored Nanocelluloses. *Langmuir* **2014**, *30* (31), 9327–9335. https://doi.org/10.1021/la5017577.
(19) He, Y. Preparation of Polyaniline/Nano-ZnO Composites via a Novel Pickering Emulsion Route. *Powder Technol.* **2004**, *147* (1–3), 59–63. https://doi.org/10.1016/j.powtec.2004.09.038.
(20) Liu, H.; Wang, C.; Gao, Q.; Chen, J.; Liu, X.; Tong, Z. One-Pot Fabrication of Magnetic Nanocomposite Microcapsules. *Mater. Lett.* **2009**, *63* (11), 884–886. https://doi.org/10.1016/j.matlet.2009.01.034.
(21) Bon, S. A. F.; Colver, P. J. Pickering Miniemulsion Polymerization Using Laponite Clay as a Stabilizer. *Langmuir* **2007**, *23* (16), 8316–8322. https://doi.org/10.1021/la701150q.
(22) Kedzior, S. A.; Marway, H. S.; Cranston, E. D. Tailoring Cellulose Nanocrystal and Surfactant Behavior in Miniemulsion Polymerization. *Macromolecules* **2017**, *50* (7), 2645–2655. https://doi.org/10.1021/acs.macromol.7b00516.
(23) Werner, A.; Sèbe, G.; Héroguez, V. A New Strategy to Elaborate Polymer Composites via Pickering Emulsion Polymerization of a Wide Range of Monomers. *Polym. Chem.* **2018,** *9***,** 5043-5050. https://doi.org/10.1039/C8PY01022F.
(24) Meng, T.; Gao, X.; Zhang, J.; Yuan, J.; Zhang, Y.; He, J. Graft Copolymers Prepared by Atom Transfer Radical Polymerization (ATRP) from Cellulose. *Polymer* **2009**, *50* (2), 447–454. https://doi.org/10.1016/j.polymer.2008.11.011.
(25) Labet, M.; Thielemans, W. Improving the Reproducibility of Chemical Reactions on the Surface of Cellulose Nanocrystals: ROP of ε-Caprolactone as a Case Study. *Cellulose* **2011**, *18* (3), 607–617. https://doi.org/10.1007/s10570-011-9527-x.
(26) Zoppe, J. O.; Venditti, R. A.; Rojas, O. J. Pickering Emulsions Stabilized by Cellulose Nanocrystals Grafted with Thermo-Responsive Polymer Brushes. *J. Colloid Interface Sci.* **2012**, *369* (1), 202–209. https://doi.org/10.1016/j.jcis.2011.12.011.
(27) Tang, J.; Berry, R. M.; Tam, K. C. Stimuli-Responsive Cellulose Nanocrystals for Surfactant-Free Oil Harvesting. *Biomacromolecules* **2016**, *17* (5), 1748–1756. https://doi.org/10.1021/acs.biomac.6b00144.
(28) Chen, T.; Colver, P. J.; Bon, S. A. F. Organic-Inorganic Hybrid Hollow Spheres Prepared from TiO 2-Stabilized Pickering Emulsion Polymerization. *Adv. Mater.* **2007**, *19* (17), 2286–2289. https://doi.org/10.1002/adma.200602447.
(29) Wu, M.; Forero Ramirez, L. M.; Rodriguez Lozano, A.; Quémener, D.; Babin, J.; Durand, A.; Marie, E.; Six, J.-L.; Nouvel, C. First Multi-Reactive Dextran-Based Inisurf for Atom Transfer Radical Polymerization in Miniemulsion. *Carbohydr. Polym.* **2015**, *130*, 141–148. https://doi.org/10.1016/j.carbpol.2015.05.002.

(30) Chen, Y.; Wang, C.; Chen, J.; Liu, X.; Tong, Z. Growth of Lightly Crosslinked PHEMA Brushes and Capsule Formation Using Pickering Emulsion Interface-Initiated ATRP. *J. Polym. Sci. Part Polym. Chem.* **2009**, *47* (5), 1354–1367. https://doi.org/10.1002/pola.23244.
(31) Bondeson, D.; Mathew, A.; Oksman, K. Optimization of the Isolation of Nanocrystals from Microcrystalline Cellulose by Acid Hydrolysis. *Cellulose* **2006**, *13* (2), 171. https://doi.org/10.1007/s10570-006-9061-4.
(32) Brand, J.; Pecastaings, G.; Sèbe, G. A Versatile Method for the Surface Tailoring of Cellulose Nanocrystal Building Blocks by Acylation with Functional Vinyl Esters. *Carbohydr. Polym.* **2017**, *169*, 189–197. https://doi.org/10.1016/j.carbpol.2017.03.077.
(33) AGET ATRP in the Presence of Air in Miniemulsion and in Bulk. *Macromol. Rapid Commun.* **2006**, *27* (8), 594–598. https://doi.org/10.1002/marc.200600060.
(34) Morandi, G.; Heath, L.; Thielemans, W. Cellulose Nanocrystals Grafted with Polystyrene Chains through Surface-Initiated Atom Transfer Radical Polymerization (SI-ATRP). *Langmuir* **2009**, *25* (14), 8280–8286. https://doi.org/10.1021/la900452a.
(35) Tesch, S.; Gerhards, C.; Schubert, H. Stabilization of Emulsions by OSA Starches. *J. Food Eng.* **2002**, *54* (2), 167–174. https://doi.org/10.1016/S0260-8774(01)00206-0.
(36) Zhang, Z.; Tam, K. C.; Wang, X.; Sèbe, G. Inverse Pickering Emulsions Stabilized by Cinnamate Modified Cellulose Nanocrystals as Templates To Prepare Silica Colloidosomes. *ACS Sustain. Chem. Eng.* **2018**, *6* (2), 2583–2590. https://doi.org/10.1021/acssuschemeng.7b04061.
(37) Zhang, Z.; Tam, K. C.; Sèbe, G.; Wang, X. Convenient Characterization of Polymers Grafted on Cellulose Nanocrystals via SI-ATRP without Chain Cleavage. *Carbohydr. Polym.* **2018**, *199*, 603–609. https://doi.org/10.1016/j.carbpol.2018.07.060.
(38) Finkle, P.; Hildebrand, J. H. The Theory of Emulsification. *Journal of American Chemical Society*. 1923, pp 2780–2788.
(39) Destribats, M.; Gineste, S.; Laurichesse, E.; Tanner, H.; Leal-Calderon, F.; Héroguez, V.; Schmitt, V. Pickering Emulsions: What Are the Main Parameters Determining the Emulsion Type and Interfacial Properties? *Langmuir* **2014**, *30* (31), 9313–9326. https://doi.org/10.1021/la501299u.
(40) Arditty, S.; Whitby, C. P.; Binks, B. P.; Schmitt, V.; Leal-Calderon, F. Some General Features of Limited Coalescence in Solid-Stabilized Emulsions. *Eur. Phys. J. E - Soft Matter* **2003**, *11* (3), 273–281. https://doi.org/10.1140/epje/i2003-10018-6.
(41) Bombalski, L.; Min, K.; Dong, H.; Tang, C.; Matyjaszewski, K. Preparation of Well-Defined Hybrid Materials by ATRP in Miniemulsion. *Macromolecules* **2007**, *40* (21), 7429–7432. https://doi.org/10.1021/ma071408k.
(42) Min, K.; Gao, H.; Matyjaszewski, K. Preparation of Homopolymers and Block Copolymers in Miniemulsion by ATRP Using Activators Generated by Electron Transfer (AGET). *J. Am. Chem. Soc.* **2005**, *127* (11), 3825–3830. https://doi.org/10.1021/ja0429364.
(43) Gillies, M. B.; Matyjaszewski, K.; Norrby, P.-O.; Pintauer, T.; Poli, R.; Richard, P. A DFT Study of R−X Bond Dissociation Enthalpies of Relevance to the Initiation Process of Atom Transfer Radical Polymerization. *Macromolecules* **2003**, *36* (22), 8551–8559. https://doi.org/10.1021/ma0351672.
(44) Drappier, C. Biofunctional self-assemblies from polymer-b-peptide conjugates, Bordeaux: Bordeaux, 2013.